

Deoxyhypusine synthase mutations alter the post-translational modification of eukaryotic initiation factor 5A resulting in impaired human and mouse neural homeostasis

Leah R. Padgett,¹ Mollie R. Shinkle,² Spencer Rosario,³ Tracy Murray Stewart,⁴ Jackson R. Foley,⁴ Robert A. Casero, Jr.,⁴ Myung Hee Park,⁵ Wendy K. Chung,⁶ and Teresa L. Mastracci^{2,7,8,9,*}

Summary

DHPS deficiency is a rare genetic disease caused by biallelic hypomorphic variants in the *Deoxyhypusine synthase* (*DHPS*) gene. The DHPS enzyme functions in mRNA translation by catalyzing the post-translational modification, and therefore activation, of eukaryotic initiation factor 5A (eIF5A). The observed clinical outcomes associated with human mutations in *DHPS* include developmental delay, intellectual disability, and seizures. Therefore, to increase our understanding of this rare disease, it is critical to determine the mechanisms by which mutations in *DHPS* alter neurodevelopment. In this study, we have generated patient-derived lymphoblast cell lines and demonstrated that human *DHPS* variants alter DHPS protein abundance and impair enzyme function. Moreover, we observe a shift in the abundance of the post-translationally modified forms of eIF5A; specifically, an increase in the nuclear localized acetylated form (eIF5A^{AcK47}) and concomitant decrease in the cytoplasmic localized hypusinated form (eIF5A^{HYP}). Generation and characterization of a mouse model with a genetic deletion of *Dhps* in the brain at birth shows that loss of hypusine biosynthesis impacts neuronal function due to impaired eIF5A^{HYP}-dependent mRNA translation; this translation defect results in altered expression of proteins required for proper neuronal development and function. This study reveals new insight into the biological consequences and molecular impact of human DHPS deficiency and provides valuable information toward the goal of developing treatment strategies for this rare disease.

Introduction

Deoxyhypusine synthase (DHPS) deficiency is a rare, autosomal recessive disorder characterized by biallelic pathogenic variants in the *DHPS* gene that are associated with neurodevelopmental issues including seizures, developmental delay/intellectual disability, and hypotonia.¹ To date, five affected individuals from four unrelated families have been identified. All of these affected individuals share one *DHPS* variant, a missense variant (c.518A>G [p.Asn173Ser]), in *trans* with a second *DHPS* variant that is either a splice site variant (c.1014+1G>A), an in-frame deletion (c.912_917_delTTACAT [p.Tyr305_Ile306del]), or a nucleotide change that disrupts the initiation codon (c.1A>G [p.Met1?]). The splice site and initiation codon variants are predicted to disrupt proper DHPS protein synthesis and thus enzyme activity.¹ Moreover, previous studies determined that the *DHPS* in-frame deletion results in an inactive enzyme, and the missense p.N173S variant causes a significant reduction in enzyme activity (approximately 18%–25% of normal).¹ These data, in combination with a shared clinical phenotype, support the clinical condition now called DHPS deficiency.¹ The discovery that human *DHPS* mutations have severe clinical consequences

on human health supports the need to identify the biological pathways downstream of DHPS.

DHPS is an enzyme that biologically connects polyamine metabolism with hypusine biosynthesis, two pathways that are essential for life.^{2–4} Polyamines are involved in many cellular functions related to growth and proliferation,^{5–7} and hypusine biosynthesis is critical for mRNA translation.^{8–13} DHPS bridges these two pathways by using the polyamine spermidine to catalyze the first step in the biosynthesis of hypusine, a post-translationally modified lysine found exclusively at position 50 in eukaryotic initiation factor 5A (eIF5A). Hypusine biosynthesis is a two-step reaction that first requires DHPS to catalyze production of the deoxyhypusine residue, and this intermediate is then hydroxylated by deoxyhypusine hydroxylase to form the hypusine residue.^{14,15} The hypusinated form of eIF5A (eIF5A^{HYP}) was first identified as an mRNA translation initiation factor^{16,17}; however, more recent studies suggest a functional role also in translation elongation and termination.^{10–12} Given that DHPS uses the polyamine spermidine for the formation of hypusine, it is plausible that altered DHPS enzyme activity could indirectly impact spermidine levels and thus initiate a polyamine imbalance. Regulation of polyamine levels is critical as they function in numerous

¹Indiana Biosciences Research Institute, Indianapolis, IN 46202, USA; ²Department of Biology, Indiana University Purdue University Indianapolis, Indianapolis, IN 46202, USA; ³Department of Biostatistics and Bioinformatics, Roswell Park Comprehensive Cancer Center, Buffalo, NY 14203, USA; ⁴Sidney Kimmel Comprehensive Cancer Center, Johns Hopkins University School of Medicine, Baltimore, MD 21231, USA; ⁵National Institute of Dental and Craniofacial Research, National Institutes of Health, Bethesda, MD 20892-4340, USA; ⁶Departments of Pediatrics and Medicine, Columbia University, New York, NY 10032, USA; ⁷Department of Biochemistry and Molecular Biology, Indiana University School of Medicine, Indianapolis, IN 46202, USA; ⁸Center for Diabetes and Metabolic Diseases, Indiana University School of Medicine, Indianapolis, IN 46202, USA

⁹Lead contact

*Correspondence: tmastrac@iu.edu

<https://doi.org/10.1016/j.xhgg.2023.100206>

© 2023 The Authors. This is an open access article under the CC BY-NC-ND license (<http://creativecommons.org/licenses/by-nc-nd/4.0/>).



cellular pathways including ion channel regulation, chromatin structure, and microtubule formation.^{18,19} Similarly, proper maintenance of the hypusine biosynthesis pathway is needed in the cell as it functions in mRNA translation and, if disrupted, can result in catastrophic effects. In particular, whole-body genetic deletion of *Dhps* or *Eif5a* is embryonic lethal in mice,^{2,3,20} and conditional deletion of *Dhps* in the mouse has been reported to directly disrupt mRNA translation in both the pancreas and brain.^{13,21,22} Whereas genetic studies demonstrate the essential function of DHPS in the null setting, the cellular consequences of reduced DHPS abundance or impaired DHPS activity in mouse models and human disease were until recently unknown.

The most severe clinical characteristics documented for patients with DHPS deficiency relate to brain development and function.¹ Interestingly, DHPS and eIF5A^{HYP} have been shown *in vitro* to be critical for neurite outgrowth and survival of PC12 cells as well as mammalian brain neurons.²³ Moreover, a study by Kar et al.²² generated mouse models of *Dhps* or *Eif5a* genetic deletion in specific brain regions and observed impaired growth, viability, neurodevelopment, and cognitive functions. In general, whole-body and cell-specific mouse models of *Dhps* loss reveal severe outcomes on the growth of organs^{2,3,13,21,22}; however, the clinical manifestation of human DHPS mutations (as observed in DHPS deficiency) is less severe with respect to growth but demonstrates a greater impact on cellular function. Therefore, there is a gap in our understanding of the functional outcomes related to reduced DHPS activity compared with complete genetic loss of *Dhps*. To begin to resolve the neurological, developmental, and metabolic outcomes associated with human DHPS deficiency, it is necessary to first determine the biological consequences of heterozygous and biallelic DHPS mutations on cellular pathways related to growth.

In this study, we present the first characterization of lymphoblast cell lines (LCLs) derived from individuals with DHPS deficiency and their clinically unaffected family members (DHPS mutation carriers). Using these patient-derived LCLs, we evaluated the effect of DHPS mutations on protein and gene expression. Moreover, we performed high-performance liquid chromatography (HPLC) to determine the effect of DHPS mutations on cellular polyamine balance as well as two-dimensional (2D) gel electrophoresis to determine changes in abundance of the hypusinated and acetylated forms of eIF5A. To identify the biologically relevant molecular signatures associated with the pathogenesis of DHPS deficiency, we generated a brain-specific deletion of *Dhps* in mouse and performed ribosome profiling and quantitative mass spectrometry to determine the impact of DHPS loss on mRNA translation and protein synthesis in the brain. This study reveals new insight into the biological consequences and molecular impacts of human DHPS deficiency and provides valuable information toward the goal of developing treatment strategies for this understudied, rare disease.

Materials and methods

Cell culture

LCLs were generated from three unrelated individuals with biallelic DHPS mutations (clinically affected), five of their relatives with heterozygous DHPS mutations (clinically unaffected) and two unrelated controls (no identified DHPS mutations). In brief, 10 mL of peripheral blood was mixed with 10 mL of phosphate-buffered saline (PBS) followed by the careful underlay of 10 mL of Ficoll-PaquePLUS (Pharmacia Biotech). The samples were centrifuged at $400 \times g$ for 30 min at room temperature. The interphase containing the peripheral blood lymphocytes was collected and washed two times with 40 mL of PBS and centrifuged each time at 100 rcf for 10 min. The cells were counted using a hemacytometer and $3\text{--}5 \times 10^6$ cells were pelleted at 100 rcf. The pelleted cells were resuspended in 3 mL of EBV supernatant and incubated in the upright position overnight at 37°C, 5% CO₂. After 24 h, 7 mL of transformation medium (RPMI 1640 + 20% FBS + 200 ng/mL cyclosporin) was added, and the cells were maintained for approximately 2–5 weeks or until transformation was achieved. The cell lines were expanded and frozen down for future use.

Upon thawing cell stocks, the transformed LCLs were maintained at 37°C, 5% CO₂ in IMDM (Gibco, no. 12440-053) supplemented with 15% FBS (Gibco, no. 26140-079), 1% penicillin-streptomycin (Gibco, no. 1510-122), 4 mM L-glutamine (Gibco, no. 25030-081), 1% amphotericin B (Sigma, A2942), 1% nystatin suspension (Sigma, no. N1638), and 100 µg/mL normocin (InvivoGen, ant-nr-1). Cells were maintained at a concentration between 6×10^5 and 1.5×10^6 cells/mL. For all experimental studies, cells were collected at three separate passages with a similar concentration of $1\text{--}1.5 \times 10^6$ cells/mL.

HEK293T cells (ATCC, no. CRL-3216) were cultured in Dulbecco's modified Eagle's medium (DMEM) supplemented with 10% HyClone FBS (Thermo Fisher Scientific, SH3091003), 1% penicillin/streptomycin, and 2 mM L-glutamine.

Protein extraction and western blot analysis

For LCL protein analysis, approximately 10 million cells were lysed in 500 µL of buffer containing 50 mM Tris (pH 8.0), 150 mM NaCl, 0.05% deoxycholate, 0.1% IGEPAL CA-630, 0.1% SDS, 0.2% sarcosyl, 10% glycerol, 1 mM DTT, 1 mM EDTA, 10 mM NaF, protease inhibitors (Roche, no. 11836170001), phosphatase inhibitors (Roche, no. 4906845001), 2 mM MgCl₂, and 0.05% (v/v) Benzonase (Millipore) and subjected to intermittent vortexing to facilitate protein extraction. Protein was quantified using the DC Protein Assay Kit II (Bio-Rad, no. 5000112) followed by SDS-PAGE (4%–20% gel). Separated protein (20 µg) was transferred to PVDF membranes and blocked in Odyssey Blocking Buffer (LI-COR Biosciences, no. 927-40100) at room temperature for 1 h. Membranes were incubated with REVERT (LI-COR Biosciences, no. 926-11016) to permit visualization of total protein. Subsequent incubation with primary antibodies diluted in Intercept Blocking Buffer (LI-COR Biosciences, no. 927-70001) was performed overnight at 4°C. Membranes were washed three times with TBST buffer prior to incubation with near infrared, fluorescent dye-conjugated secondary antibodies at room temperature for 1 h. Following three washes with TBST buffer, the membranes were imaged using an Odyssey CLx Imaging System and images were analyzed using the CLx Image Studio v.5.2 software (LI-COR Biosciences).

The following primary antibodies were used at the dilutions indicated: mouse anti-deoxyhypusine synthase (1:2,000, Santa Cruz, no. sc-365077), rabbit anti- β -tubulin (1:2,000, Cell Signaling Technology, no. 2146S), mouse anti-eIF5A (1:2,000, BD Biosciences, no. 611977), rabbit anti-acetylated eIF5A (eIF5A^{AcK47}) (1:2,000; Booster Bio, no. P01727), and rabbit anti-hyposinated eIF5A (eIF5A^{HYP}) (1:2,000, Maier et al.²⁴), chicken anti-GFP (1:2,000, Aves Labs, no. GFP-1020), and goat anti-HA (1:2,000, Novus Technologies, no. NB600362). Densitometric data are graphed as relative expression, and statistical significance was determined using a one-way ANOVA (Prism 9, GraphPad).

Protein stability assays

For initial assessment of DHPS stability, we created GFP fusion constructs expressing either wild-type DHPS (GFP^{WT}DHPS) or DHPS containing the deletion mutation (Y305_I306 DHPS; GFP^{DEL}DEL). Using the previously described wild-type (DHPS) and DHPS-deletion (DEL) constructs as DNA templates,¹ we amplified the corresponding DHPS or DEL sequences starting with the start codon through the stop codon using the DHPS-GFP-forward: 5'-CGAATTCTG CAGTCGACATGGAAGGTTCCCTGGAACG-3' and DHPS-GFP-reverse: 5'-GATCCGGTGGATCCCTCAGTCCTGTTCTTCTCATG CATGA-3' primers. These amplicons were inserted into the pEGFP-C1 plasmid¹ at the *AccI* and *SmaI* sites using the In-Fusion HD cloning kit (Takara Bio). The open reading frame for each construct was Sanger sequenced using the following primers: 5'-CGACCACTAC CAGCAGAACA-3' and 5'-AGCACAACATGGTGGACGTA-3'.

HEK293T cells were grown to 60%–70% confluency (~300,000 cells/well, 6-well plate) and transiently transfected using Lipofectamine 3000 (Invitrogen, no. L3000008) with 500 ng of GFP or HA-tagged DHPS DNA constructs (GFP^{WT}DHPS, HA^{WT}DHPS, GFP^{DEL}DEL, or HA^{DEL}DEL; previously published in Ganapathi et al.¹). At 24 h after transfection, cells were washed with PBS and incubated with 200 μ L of lysis buffer on ice. Western blot analysis was performed as described above.

To assess protein stability over time, GFP^{WT}DHPS and GFP^{DEL}DEL constructs (100 ng) were transiently transfected into HEK293T cells as described above. At 18 h post-transfection, cells were treated with the proteasome inhibitor MG132 (5 μ M) followed by treatment with cyclohexamide (CHX) (20 μ g/mL) at various times (0, 0.5, 1, 2, 4, and 6 h). At 24 h, cells were lysed and subjected to western blot analysis. Densitometric data are shown as percent over time and statistical significance was determined using a two-way ANOVA (Prism 9, GraphPad).

Quantitative RT-PCR

For each human-derived LCL, total RNA was isolated from approximately 10 million cells using the RNeasy Plus Mini Kit (QIAGEN, no. 74134). An on-column DNaseI treatment was performed to eliminate any possible DNA contamination. High RNA quality was confirmed using the TapeStation System (Agilent). For qRT-PCR analysis, RNA was converted to cDNA using the SuperScript VILO Master Mix (Thermo Scientific, cat no. 11755050) and then subjected to Real-Time PCR using a Quantstudio3 real-time PCR machine (Thermo Fisher Scientific), PowerUp SYBR Green Master Mix (Thermo Fisher Scientific, no. A25742), and oligonucleotide primers specific to human DHPS (DHPS-forward: 5'-GGA GAACGGGATCAATAGGA-3', DHPS-reverse: 5'-TCATCTAGAAG GCGTCCAC-3') and β -tubulin (*beta-tubulin*-forward: 5'-CTACCT CCCTCACTCAGCT-3', *beta-tubulin*-reverse: 5'-CAGAGTCAGGG GTGTTTCAT-3') as a control. Transcript abundance was calculated

(Δ/Δ CT) and statistical significance was determined using a one-way ANOVA (Prism 9, GraphPad).

2D gel analysis

Sample preparation was adapted from previous publications.^{25–27} In brief, approximately 10 million cells were collected from each LCL to be analyzed, washed with PBS, lysed in 2-D cell lysis buffer (Applied Biomix) and quantified for protein concentration (Bio-Rad). Control and experimental samples were labeled with either Cy3 or Cy5 dyes. For each sample, 30 μ g of protein was mixed with 1 μ L of diluted CyDye; the labeling reaction was stopped by adding 1 mL of 10 mM lysine to each sample. The labeled samples were mixed together and separated by IEF (pH 3–10) (GE Healthcare) followed by SDS-PAGE gels (12% at 15°C) (Bio-Rad). Gel images were scanned using Typhoon TRIO (GE Healthcare) and analyzed by Image Quant software v.6.0 (GE Healthcare), followed by cross-gel analysis using DeCyder software v.6.5 (GE Healthcare). Spot locations for all forms of eIF5A were subsequently identified by western blot using an eIF5A antibody (BD Biosciences, no. 611977) that recognizes all three forms: eIF5A hypusinated at K50 (eIF5A^{HYP}), eIF5A unhyposinated at lysine 50 (eIF5A^{K50}), and eIF5A unhyposinated at K50 but acetylated at lysine 47 (eIF5A^{K50/AcK47}). Densitometric analysis of eIF5A^{HYP}, eIF5A^{K50}, and eIF5A^{K50/AcK47} was performed using Image Studio software (LI-COR Biosciences). The quantified amount of each form of eIF5A was presented as a percentage of the total of all forms of eIF5A (eIF5A^{HYP} + eIF5A^{K50} + eIF5A^{K50/AcK47}).

Polyamine analysis

For each human-derived LCL, approximately 10 million cells were collected, washed with PBS, lysed, and then measured for the concentration of intracellular polyamines using the pre-column derivatization, reverse-phase HPLC methods described previously.²⁸ The polyamines putrescine, spermidine, and spermine were measured. The data are represented in two ways: (1) the quantity of each polyamine shown as a proportion (%) of the total amount of all three polyamines and (2) quantity (nmol) of each polyamine per mg of protein. Statistical significance was determined using a one-way ANOVA (Prism 9, GraphPad).

Animal studies

Animals were maintained under a protocol approved by both the Indiana University School of Medicine and Indiana University-Purdue University-Indianapolis (IUPUI) School of Science Institutional Animal Care and Use Committees. Mice containing both the *Dhps*^{loxP} allele (B6.Cg-Dhps^{tm1.1Mirm/J})²¹ and *R26R*^{Tomato} reporter allele (B6.Cg-Gt(Rosa)26Sor^{tm14(CAG-tdTomato)Hze/J})²⁹ were maintained on an outbred, mixed background. Timed matings were established; noon on the day of appearance of a vaginal plug was considered embryonic day 0.5. On postnatal day 0 (P0) (the day of birth), all pups in a litter were anesthetized and then subjected to intraventricular injection with 4 μ L of self-complementary adeno-associated virus 2/9 (scAAV2/9), with a CMV (cytomegalovirus) promoter driving the expression of Cre recombinase (scAAV2/9-CMV-Cre; 9.6e+12 vg/mL; University of Iowa Viral Vector Core, no. AAV3558) combined with 1 μ L of trypan blue (Thermo Fisher Scientific, no. 12-250-061). The injected virus will migrate immediately and within 24 h spread throughout the ventricle. The virus can infect any cell in the brain. In the cells where Cre recombinase becomes expressed (viral infected cells), *Dhps* will be genetically deleted if the *Dhps*^{loxP} allele(s) are present in that animal. In addition, in the Cre-expressing cells, the

R26R^{Tomato} reporter will also be expressed. Therefore, expression of Tomato fluorescence is used as a marker of Cre-expressing cells as well as a reporter for *Dhps* deletion.

Following intraventricular injection, animals were tattooed (Thermo Fisher Scientific, no. NC9665212) for identification and genotyped by PCR using primers described previously.^{21,29} At weaning (age 3 weeks), animal weight and blood glucose levels were measured using a digital scale (Thermo Fisher Scientific), and AlphaTrak2 glucose monitor and test strips (Thermo Fisher Scientific), respectively. Animal weight and viability were then followed weekly through to 6 weeks of age. Adult mouse brain tissue was dissected; whole-mount images were acquired using a Leica M205 fluorescent dissecting microscope to confirm Tomato expression (from the *R26R^{Tomato}*) and thus Cre activity. Brain tissue was also processed for western blot analysis, as described above, to confirm *Dhps* knockdown. Moreover, additional whole brains were harvested, fixed using 4% paraformaldehyde (Acros Organics), cryo-preserved in 30% sucrose (Thermo Fisher Scientific), embedded in OCT (Thermo Fisher Scientific), and sectioned (15 μ m, coronal) using a CM1950 Cryostat (Leica). Sections were stained with the nuclear marker DAPI (1:1,000, Sigma) and tile scanned at 10 \times magnification on a C2 confocal microscope (Nikon) to identify the endogenous tomato-expressing cells. Image analysis was performed using QuPath software v.0.4.1.³⁰ Cell detection used the default parameters for the 405 channel (DAPI) and a cell expansion value of 10 μ m. An object filter was then set to identify cells in the dTomato channel (*R26R^{Tomato}* reporter); the measurement was set as “cell:dTomato mean” with a threshold of 350. All cells above the threshold were designated positive (Tomato expressing) and graphed as the percentage of the total number of detected cells (DAPI).

Ribosome profiling

Ribosome profiling experiments were performed as described previously.^{13,31} In brief, cell lysate from mouse brain tissue was passed through a 10%–50% sucrose gradient and fractionated using a piston gradient fractionator (BioComp Instruments). Absorbance at 254 nm was recorded using an in-line UV monitor (BioComp Instruments). Polyribosome to monoribosome (P/M) ratios were determined by calculating the area under the curve corresponding to the polyribosome peaks (more than two ribosomes) divided by the area under the curve for the monoribosome (80S) peak.

TMT labeling and mass spectrometry

Whole mouse brain tissue from 3-week-old wild-type and *Dhps^{loxP/loxP}* animals injected with scAAV2/9-CMV-Cre at birth was dissected and processed for analysis by mass spectrometry. Brain tissues were lysed in 8 M urea (CHEBI: 16199), 100 mM Tris-HCl (pH 8.5) (CHEBI: 975446756, Sigma-Aldrich cat. no. 10812846001) by sonication in 1.5 mL Micro Tubes (TPX Plastic for Sonication from Diagenode) using a Bioruptor sonication system (Diagenode, no. B01020001) with 30 s/30 s on/off cycles for 15 min in a water bath at 4°C. After subsequent centrifugation at 14,000 rcf for 20 min, protein concentrations were determined by Bradford protein assay (Bio-Rad, no. 5000006). The global proteomics workflow used 25 μ g equivalent of protein from each sample. Proteins were reduced with 5 mM tris(2-carboxyethyl) phosphine hydrochloride (Sigma-Aldrich, no. C4706) for 30 min at room temperature and the resulting free cysteine thiols were alkylated with 10 mM chloroacetamide (Sigma Aldrich, no. C0267) for 30 min at room temperature in the dark. Samples were diluted with 50 mM Tris-HCl (pH 8.5) to a final urea concentration of 2 M for

Trypsin/Lys-C-based overnight protein digestion at 37°C (1:70 protease:substrate ratio, mass spectrometry grade, Promega, no. V5072).

Digestions were acidified with trifluoroacetic acid (TFA) (0.5% v/v) and desalted on Sep-Pak Vac cartridges (Waters, no. WAT054955) with a wash of 1 mL 0.1% TFA followed by elution in 70% acetonitrile and 0.1% formic acid (FA). Peptides for the global experiments were dried by speed vacuum and resuspended in 24 μ L of 50 mM triethylammonium bicarbonate. Peptide concentrations were checked by Pierce Quantitative colorimetric assay (cat. no. 23275). The same amount of peptide from each sample was then labeled for 2 h at room temperature, with 0.2 mg of a tandem mass tag (TMT) reagent (Thermo Fisher Scientific, TMT Isobaric Label Reagent Set, no. 90110). Labeling reactions were quenched by adding 0.2% hydroxylamine final v/v to the reaction mixtures at room temperature for 15 min. Labeled peptides were then mixed and dried by speed vacuum.

For high pH basic fractionation, peptides were reconstituted in 0.1% trifluoroacetic acid and fractionated on Sep-Pak Vac cartridges using methodology and reagents from Pierce High pH reversed-phase peptide fractionation kit (eight fractions for each peptide mixture; Thermo Fisher Scientific, no. A32993).

Nano-LC-MS/MS analyses were performed on an EASY-nLC HPLC system (SCR: 014993, Thermo Fisher Scientific) coupled to an Orbitrap Lumos Tribrid mass spectrometer (Thermo Fisher Scientific). One-eighth of each global peptide fraction was loaded onto a reversed-phase EasySpray C18 column (2 μ m, 100 \AA , 75 μ m \times 25 cm, Thermo Scientific, no. ES902A) at 400 nL/min. Peptides were eluted from 4% to 30% with mobile phase B (mobile phases A: 0.1% FA, water; B: 0.1% FA, 80% acetonitrile) (Thermo Fisher Scientific, no. LS122500) over 160 min, 30%–80% B over 10 min; and dropping from 80% to 10% B over the final 10 min. The mass spectrometer was operated in positive ion mode with a 4 s cycle time data-dependent acquisition method with advanced peak determination and Easy-IC (internal calibrant). Precursor scans (m/z 400–1,750) were done with an Orbitrap resolution of 120,000, RF lens% 30, maximum inject time 50 ms, standard AGC target, MS2 intensity threshold of 2.5×10^{-4} , including charges of 2–7 for fragmentation with 30 s dynamic exclusion. MS2 scans were performed with a quadrupole isolation window of 0.7 m/z , 38% HCD CE, 50,000 resolution, 200% normalized AGC target, dynamic maximum IT fixed first mass of 100 m/z .

Resulting RAW files were analyzed in Proteome Discover 2.2 (Thermo Fisher Scientific, RRID: SCR_014477) with a *Mus musculus* UniProt FASTA (both reviewed and unreviewed sequences downloaded 01_09_2017) as required by the experiment, plus common contaminants. Quantification methods utilized isotopic purity levels available from Thermo Fisher Scientific. SEQUEST HT searches were conducted with a maximum number of three missed cleavages; precursor mass tolerance of 10 ppm; and a fragment mass tolerance of 0.02 Da. Static modifications used for the search were (1) carbamidomethylation on cysteine (C) residues, (2) TMT label on lysine (K) residues, and (3) TMT label on the N termini of peptides. Dynamic modifications used for the search were oxidation of methionines, acetylation, Met-loss, or Met-loss plus acetylation of protein of N termini. Percolator false discovery rate was set to a strict setting of 0.01 and a relaxed setting of 0.05. In the consensus workflows, unique and razor peptides were used, and samples were normalized by total peptide amount. Protein abundance-based protein ratio calculations were done with an ANOVA (individual proteins) hypothesis test. Resulting normalized abundance values for each sample type, abundance ratio, and $\log_2(\text{abundance ratio})$ values; and respective p values from Proteome Discover were exported to Microsoft Excel. The

accession number for the raw and processed mass spectrometry data reported in this paper is MassIVE: MSV000092112.

Differential protein analysis

Samples were first assessed via principal-component analysis (PCA).³² To visualize these data, we utilized the “PCAtools” package in R. To assess differential protein expression, we utilized the “limma”³³ package in R, as described previously.^{34,35} In short, limma compares pre-determined groups and produces a moderated t-statistic from the empirical Bayesian procedure, assigning both a log fold change (logFC) and p value. Differentially expressed proteins (DEPs) were deemed significant if they had a $|\logFC| > 1.5$, and a p value < 0.05 . These volcano plots were constructed using “EnhancedVolcano.” DEPs were then functionally enriched utilizing the STRING database,³⁶ to create a network and also enrich for pathways in which differential proteins appear.³⁷ The Wikipathways³⁸ plug-in for Cytoscape³⁹ was then used to integrate and visualize specific functionally enriched pathways of interest based on protein level expression. The analysis was carried out in the R environment (4.0.1) for statistical computing, which is an open source dialect of the S statistical computing language.

Results

DHPS protein expression is altered in patient-derived LCLs from individuals with DHPS deficiency

Human-derived LCLs were created from three unrelated individuals with DHPS deficiency and their clinically unaffected heterozygous family members. As we previously reported, all affected individuals share a heterozygous missense variant (c.518A>G [p.Asn173Ser]; denoted as DHPS^{MIS}) and either a splice site variant (c.1014+1G>A; denoted as DHPS^{SPLICE}), in-frame deletion (c.912_917_delTTACAT [p.Tyr305_Ile306del]; denoted as DHPS^{DEL}), or variant disrupting the initiation codon (c.1A>G [p.Met1?]; denoted as DHPS^{MET}).¹ Cell lines generated and analyzed in this study include those from affected individuals with the compound DHPS^{MIS}/DHPS^{DEL} and DHPS^{MIS}/DHPS^{SPLICE} mutations, and unaffected heterozygous mutation carrier family members (DHPS^{MIS}, DHPS^{DEL}, or DHPS^{SPLICE}); this represents individuals from three of the previously reported families (Table 1).¹ We included LCLs from two unrelated, unaffected individuals as controls (control 1 and control 2; Table 1).

To determine the effect of *DHPS* mutations on protein expression levels, western blot analysis for DHPS was performed on the total soluble protein fractions extracted from the human-derived LCLs. In the LCLs from carriers, we observed significantly reduced levels of DHPS in the presence of the DHPS^{DEL} and DHPS^{SPLICE} variants but not the DHPS^{MIS} variant (Figures 1A and 1B). In LCLs from the affected individuals, significantly reduced DHPS was observed in the presence of DHPS^{MIS}/DHPS^{DEL} but not DHPS^{MIS}/DHPS^{SPLICE} (Figures 1A and 1B). Interestingly, when the western blot membrane was subjected to a longer exposure time, we visualized DHPS protein of reduced size in the LCLs expressing the DHPS^{SPLICE} variant

(Figure 1A, arrows), which is consistent with our previous report that the DHPS^{SPLICE} mutation would alter splicing and possibly result in a truncated DHPS protein.¹

To better understand the relative effects of each mutation on DHPS protein expression, we compared DHPS protein expression from cells of related family members (Figure 1C). Across all families, the cells from individuals heterozygous for the DHPS^{MIS} variant showed no significant difference in DHPS abundance compared with control cells. In family 1, DHPS protein abundance in the DHPS^{SPLICE} carrier was significantly decreased compared with both the control cells and the cells from the DHPS^{MIS}/DHPS^{SPLICE}-affected individual. In family 2, the DHPS^{MIS}/DHPS^{DEL} cells showed a significantly reduced DHPS abundance compared with control, and the level of DHPS was intermediate between the levels observed in the DHPS^{DEL} carrier cells and the DHPS^{MIS} carrier cells. In family 3 there was no significant difference between the DHPS protein abundance from the DHPS^{MIS} variant cells compared with the DHPS^{MIS}/DHPS^{SPLICE} affected individual cells. Altogether, the most dramatic reduction in the abundance of DHPS protein was not observed in the affected individuals, reflecting that these analyses measure total protein and not total *functional* protein.

To determine if changes in protein expression result from changes in gene expression, we measured DHPS transcript abundance by quantitative real-time PCR. The results were grouped by family to permit comparison between related individuals as well as with changes in protein expression. Across all families, no significant difference was observed in the abundance of *DHPS* transcript (Figure 1D). Taken together, these data suggest that changes in DHPS protein expression do not result from reduced levels of *DHPS* transcript.

Given that DHPS uses the polyamine spermidine for the formation of hypusine, it is plausible that altered DHPS could indirectly impact spermidine levels and, thus, initiate a polyamine imbalance. With respect to polyamine biosynthesis, putrescine is processed to become spermidine, which can be subsequently processed into the polyamine spermine. To provide a complete picture of polyamine abundance in our LCLs, we used HPLC to measure all three of these polyamines and observed no significant difference in the quantity of putrescine, spermidine, or spermine in cells from controls, carriers, or affected individuals (Figure S1). These data suggest that the polyamine cofactor, spermidine, required for the hypusination of eIF5A would not be limiting in LCLs harboring *DHPS* mutations. Moreover, we can conclude that reducing DHPS function does not cause an accumulation of polyamines, including spermidine.

Loss of Tyr305 and Ile306 (DHPS^{DEL}) results in DHPS protein degradation and reduced enzyme activity

The western blot analyses identified that the DHPS^{DEL} resulted in the greatest reduction in DHPS protein expression, without change in gene expression. In line with these data, using our *in vitro* overexpression system to drive expression of individual *DHPS* variants, we consistently observed a

Table 1. Summary of lymphoblast cell lines generated from individuals with DHPS deficiency, related DHPS mutation carriers, and unrelated controls

Group	Individual	DHPS mutation(s)	Designation
Control	1	no known DHPS mutations	control 1
	2	no known DHPS mutations	control 2
Family 1	1	c.1014+1G>A	DHPS-SPLICE
	2	c.1014+1G>A	DHPS-SPLICE
	3	c.518A>G[p.Asn173Ser] and c.1014+1G>A	DHPS-MIS/DHPS-SPLICE
Family 2	1	c.912_917_delTTACAT [p.Tyr305_Ile306del]	DHPS-DEL
	2	c.518A>G[p.Asn173Ser]	DHPS-MIS
	3	c.518A>G[p.Asn173Ser] and c.912_917_delTTACAT [p.Tyr305_Ile306del]	DHPS-MIS/DHPS-DEL
Family 3	1	c.518A>G[p.Asn173Ser]	DHPS-MIS
	2	c.518A>G[p.Asn173Ser] and c.1014+1G>A	DHPS-MIS/DHPS-SPLICE

decrease in DHPS protein expression when overexpressing the GFP-tagged deletion-containing DHPS variant construct (^{GFP}DEL) as compared with the wild-type DHPS (^{GFP}DHPS) construct (equal amounts of DNA were transfected) (Figure 2A). These observations were independently confirmed using the HA-tagged deletion-containing DHPS variant construct (^{HA}DEL compared with ^{HA}DHPS) (Figure 2B). These data suggest that the loss of amino acids Tyr305 and Ile306 in the DHPS^{DEL} variant causes decreased DHPS enzyme abundance. We speculated that the loss of these two amino acids (Tyr305 and Ile306) in the DHPS^{DEL} variant may result in protein instability and degradation, thus resulting in decreased enzyme activity and reduced generation of eIF5A^{HYP}.

To explore the possibility that the DHPS^{DEL} variant contributes to DHPS protein degradation in mammalian cells, we performed a CHX chase assay. For this experiment, HEK293T cells were transiently transfected with constructs expressing GFP-tagged wild-type DHPS or deletion-containing DHPS (denoted as ^{GFP}DHPS or ^{GFP}DEL, respectively) and treated with the protein synthesis inhibitor CHX at various time points (0, 0.5, 1, 2, 4, and 6 h) to determine protein half-life. At 24 h post-transfection, cells were lysed and DHPS protein levels were measured by western blot analysis. These data identified that the ^{GFP}DEL half-life was significantly shorter than the ^{GFP}DHPS half-life (Figures 2C and 2D). Furthermore, addition of the proteasome inhibitor MG132 restored ^{GFP}DEL protein levels (Figures 2E and 2F). These data confirm that the loss of amino acids Tyr305 and Ile306 in the DHPS^{DEL} variant causes protein instability and degradation.

Mutations in DHPS alter the post-translational modification of eIF5A in human patient-derived LCLs

Our *in vitro* overexpression data (Figure 2) and previously published findings¹ demonstrate that mutations in DHPS impact enzymatic activity thus causing a reduction in the amount of hypusinated eIF5A. To determine whether these

findings translate to the human disease setting, we analyzed the patient-derived LCLs by western blot for eIF5A^{HYP} abundance. The LCLs from carriers showed no significant difference in protein abundance of eIF5A^{HYP} or total eIF5A compared with unrelated controls (Figures 3A and 3B). In the LCLs from affected individuals, the ratio of eIF5A^{HYP}/total eIF5A was not significantly different (Figures 3A and 3B). We speculated that western blot analysis may not be sensitive enough to resolve changes in abundance of different forms of eIF5A from the LCL lysates. Therefore, we used 2D gel electrophoresis to better visualize changes in eIF5A^{HYP} in LCLs. This technique can identify three forms of eIF5A: eIF5A hypusinated at K50 (eIF5A^{HYP}), eIF5A unhyposinated at lysine 50 (eIF5A^{K50}), and eIF5A unhyposinated at K50 but acetylated at lysine 47 (eIF5A^{K50/AcK47}) (Figure 3C). Using 2D gel electrophoresis, the abundance of each form of eIF5A was visualized from the LCLs of affected individuals in each family and controls. The gels showed a shift in the pattern of expression for the affected individuals compared with controls. In particular, cells carrying two mutations in DHPS showed a greater visual abundance of the acetylated form of eIF5A (eIF5A^{K50/AcK47}) compared with controls that showed nearly absent expression of eIF5A^{K50/AcK47} (Figures 3D and S2). Quantification of each form of eIF5A, relative to the total of all forms, confirmed the increase in eIF5A^{K50/AcK47} as well as identified a decrease in eIF5A^{HYP} and eIF5A^{K50} in cells from the affected individuals compared with controls (Figure 3E). Our data are in line with previously published results, which identified that impaired hypusination results in a decrease in the hypusinated form and an increase in the acetylated form of eIF5A.⁴⁰ Furthermore, this suggests that biallelic variants in DHPS result in a shift in the abundance of the post-translationally modified forms of eIF5A, such that there is an increase in the acetylated form, which is sequestered in the nucleus, and a resultant decrease in the hypusinated form that is localized and functions in the cytoplasm. Therefore, simply measuring the abundance of eIF5A^{HYP} alone may not provide a complete understanding of the impact on DHPS enzymatic activity.

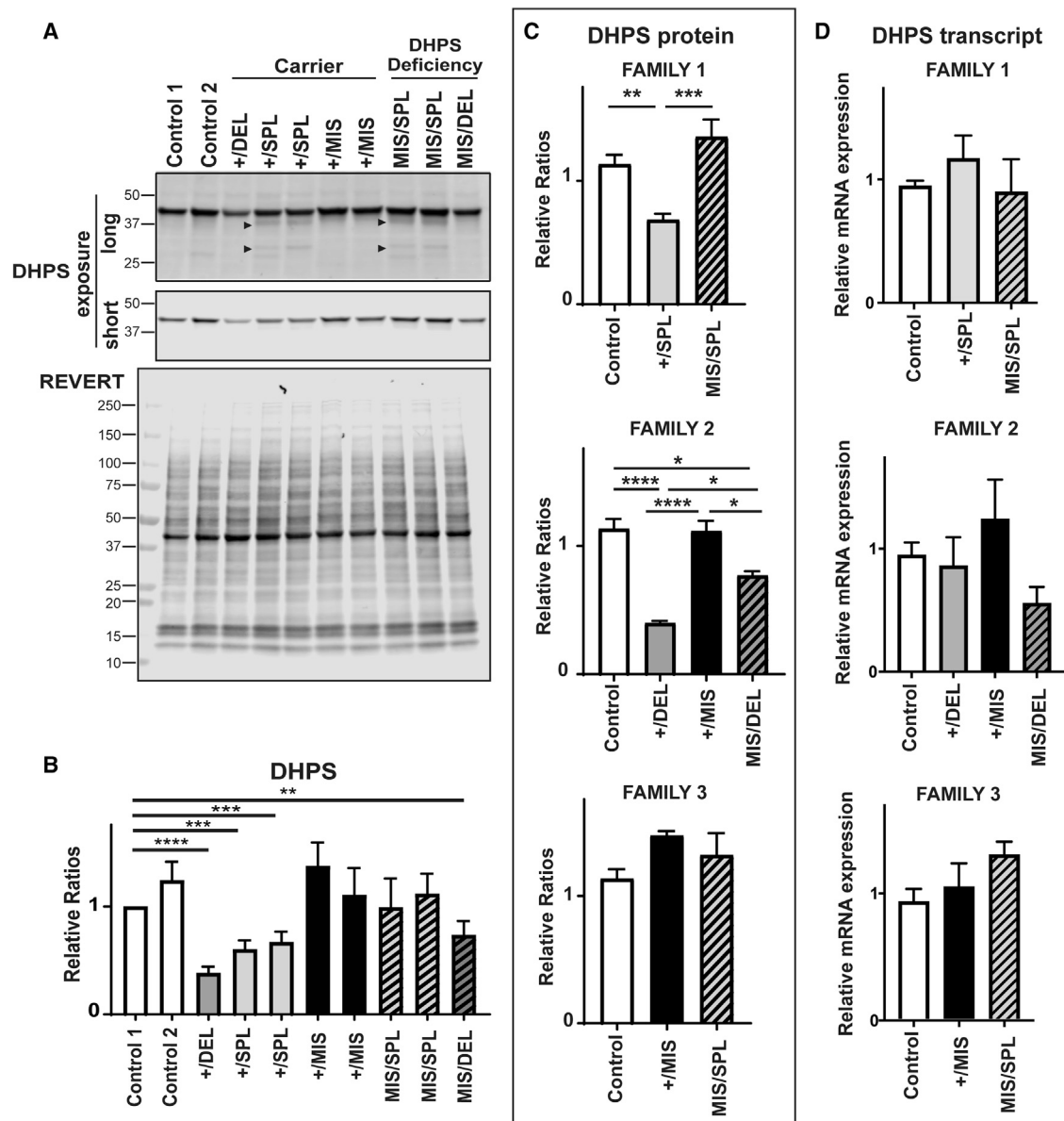


Figure 1. Analysis of DHPS in patient-derived LCLs

(A) Representative western blot analysis of LCLs from control, carrier, and affected individuals with DHPS deficiency to measure the abundance of DHPS and total protein (as visualized by REVERT). Additional DHPS isoforms are visualized in all cell lines with the DHPS^{SPL} mutation. DHPS isoforms are marked by black arrowheads. Molecular marker notations are in kDa.

(B) Relative protein levels of DHPS normalized to total protein. Data are means \pm SEM, n = 3.

(C) Relative protein levels of DHPS normalized to total protein and grouped by family (family 1, 2, and 3) to permit comparison of DHPS abundance in cell lines from related individuals.

(D) Relative mRNA expression of *DHPS* in each cell line. Data grouped by family to permit comparison between related individuals and with DHPS protein expression. Data are means \pm SEM, n = 3; *p < 0.05, **p < 0.01, ***p < 0.001, ****p < 0.0001.

Rather determining the relative amounts of each modified form of eIF5A provides critical information regarding the sub-cellular location and therefore function of eIF5A.

The absence of DHPS in the brain phenocopies clinical characteristics of human DHPS deficiency and identifies cellular changes

Individuals with DHPS deficiency show significant neurological clinical symptoms including seizures, developmental delay, and altered speech.¹ Given this documented

impact of mutant DHPS on brain function, the known role of eIF5A^{HYP} in mRNA translation,^{8–12} and our findings from patient-derived LCLs that link human *DHPS* mutations with reduced DHPS abundance and enzyme activity (Figures 1, 2, and 3), we hypothesized that loss of DHPS during brain development would impair the translation of proteins required for proper neuronal function. To test this hypothesis, we generated a mouse model wherein *Dhps* was deleted in the brain at birth. Mice harboring the *Dhps* conditional allele (*Dhps*^{loxP/loxP}; Levasseur

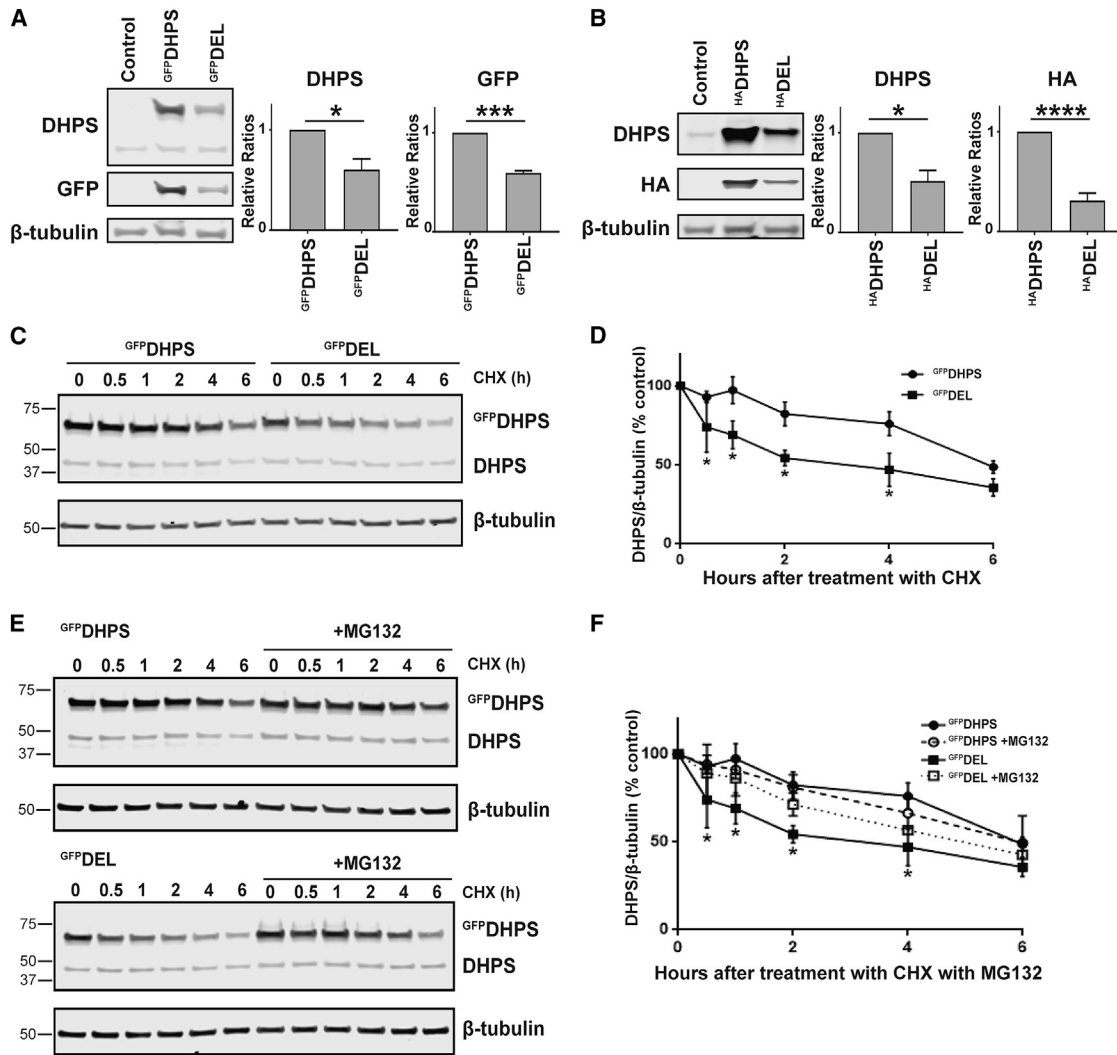


Figure 2. Deletion of amino acids Tyr305 and Ile306 results in decreased DHPS stability

HEK293T cells were transiently transfected with (A) GFP-tagged wild-type *DHPS* (or DEL) or (B) HA-tagged wild-type *DHPS* (or DEL) expression constructs (500 ng). At 24 h post-transfection, DHPS protein expression was assessed by western blot analysis; representative blots of DHPS, GFP or HA, and β -tubulin are shown. Graphical representations are included of DHPS protein expression levels normalized to the transfected DHPS control (GFP^{WT}DHPS or HA^{WT}DHPS). Data are means \pm SEM, $n = 3$; * $p < 0.05$, *** $p < 0.001$.

(C) At 18 h post-transfection, cells expressing GFP^{WT}DHPS or GFP^{DEL}DHPS fusion protein were treated with the protein synthesis inhibitor cyclohexamide (CHX) (20 μ M) and harvested at the indicated times (h). Representative western blot of DHPS and β -tubulin.

(D) Densitometric data represented as percent over time; data are means \pm SEM, $n = 3$; * $p < 0.05$.

(E) CHX chase assay performed with the proteasome inhibitor MG132 (5 μ M); a representative western blot is shown.

(F) Densitometric data represented as percent over time; data are means \pm SEM, $n = 3$; * $p < 0.05$. For all blots, β -tubulin was used as a loading control. All molecular marker notations are in kDa.

et al.²¹) and littermate controls were subjected to intraventricular injection of self-complementary (sc) AAV2/9-CMV-Cre on P0, to produce a mutant mouse model with loss of *Dhps* in the brain from birth. The *R26R^{Tomato}* allele²⁹ was used to visualize Cre-mediated recombination and showed significant reporter expression throughout the forebrain and midbrain (Figures S3A and S3B) and an absence of reporter expression in other organs (data not shown). The analysis of tissue sections from the brains of 3-week-old animals injected at birth with scAAV2/9-CMV-Cre confirmed that tomato-expressing (and therefore Cre-expressing) cells compose an average of 78%, 63%, and 65% of cells in the forebrain, anterior midbrain, and posterior

midbrain, respectively (Figures S3C–S3G). Tomato-expressing cells were not observed in the hindbrain (Figure S3H).

Whole-brain tissue was analyzed by western blot, which confirmed that scAAV2/9-CMV-Cre injection resulted in a reduction in DHPS protein expression in the injected *Dhps^{loxP/+}* animals (referred to as DHPS^{HET}), with even greater reduction in DHPS in the injected *Dhps^{loxP/loxP}* animals (referred to as DHPS^{KO}) compared with injected wild-type *Dhps^{+/+}* animals (referred to as DHPS^{WT}) (Figures 4A and 4B). The large decrease in DHPS in the DHPS^{KO} animals also resulted in a reduction of eIF5A^{HYP} expression (Figures 4A and 4B). Moreover, in line with the observed changes in the modified forms of eIF5A in the LCLs by 2D

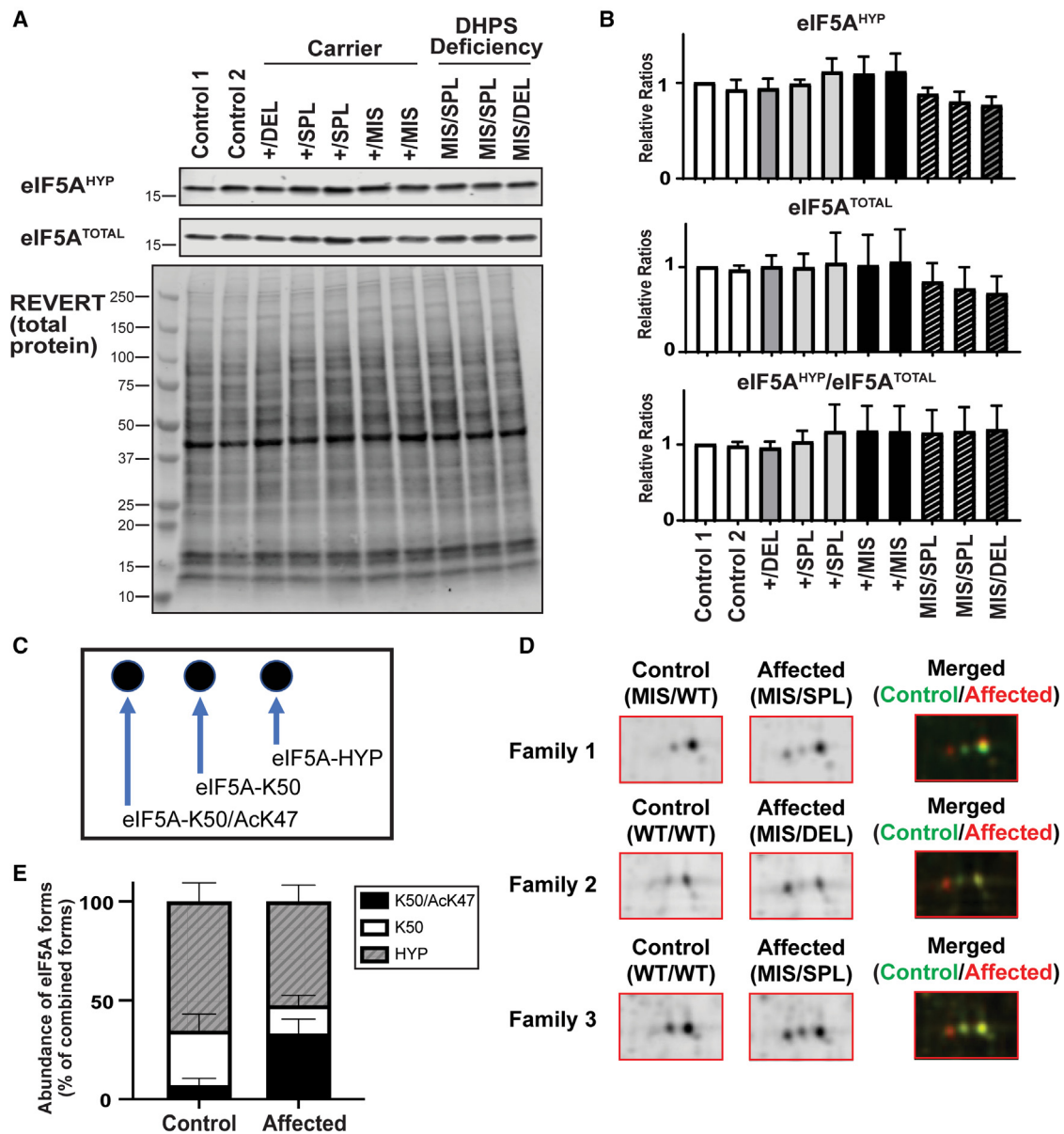


Figure 3. Analysis of patient-derived LCLs for impact of *DHPS* mutations on hypusination of eIF5A

(A) Representative western blot analysis of LCLs from control, carrier, and affected individuals with *DHPS* deficiency to assess abundance of eIF5A^{HYP}, eIF5A^{TOTAL}, and total protein (as visualized by REVERT). Molecular marker notations are in kDa.

(B) Relative protein levels of eIF5A^{HYP}, eIF5A^{TOTAL}, and the ratio of eIF5A^{HYP} to eIF5A^{TOTAL} normalized to total protein. Data are means ± SEM, n = 3; *p < 0.05.

(C) Schematic diagram of a 2D gel depicting the location of each modified form of eIF5A including hypusinated eIF5A (eIF5A^{HYP}), unhyposinated eIF5A (eIF5A-K50), and unhyposinated/acetylated eIF5A (eIF5A-K50/AcK47).

(D) Visualization by 2D gel of the three modified forms of eIF5A expressed in the LCLs from controls and affected individuals with *DHPS* deficiency.

(E) Quantification of the abundance of each form of eIF5A visualized by 2D gel; the densitometric data are mean ± SEM and represented as percent of combined forms of eIF5A.

gel, we observed a significant increase in the acetylated form, eIF5A^{AcK47} (Figures 4A and 4B). *DHPS*^{WT}, *DHPS*^{HET}, and *DHPS*^{KO} animals showed identical growth and viability from birth to age 3 weeks (Figures S4A and S4B). *DHPS*^{WT} and *DHPS*^{HET} animals received an identical intraventricular injection and titer of the scAAV2/9-CMV-Cre as *DHPS*^{KO} animals and displayed normal survival, which also confirmed that our technical methods for generating this animal model

did not result in viral toxicity (Figure 4C). In line with some of the features of *DHPS* deficiency, *DHPS*^{KO} animals displayed random seizures, stalled growth, and died before age 6 weeks (Figures 4C and S4B).

To determine the impact of loss of *DHPS* in the brain on mRNA translation, we used ribosome profiling to evaluate brain tissue from 3-week-old animals. This age was chosen due to the identical growth and normal metabolism observed

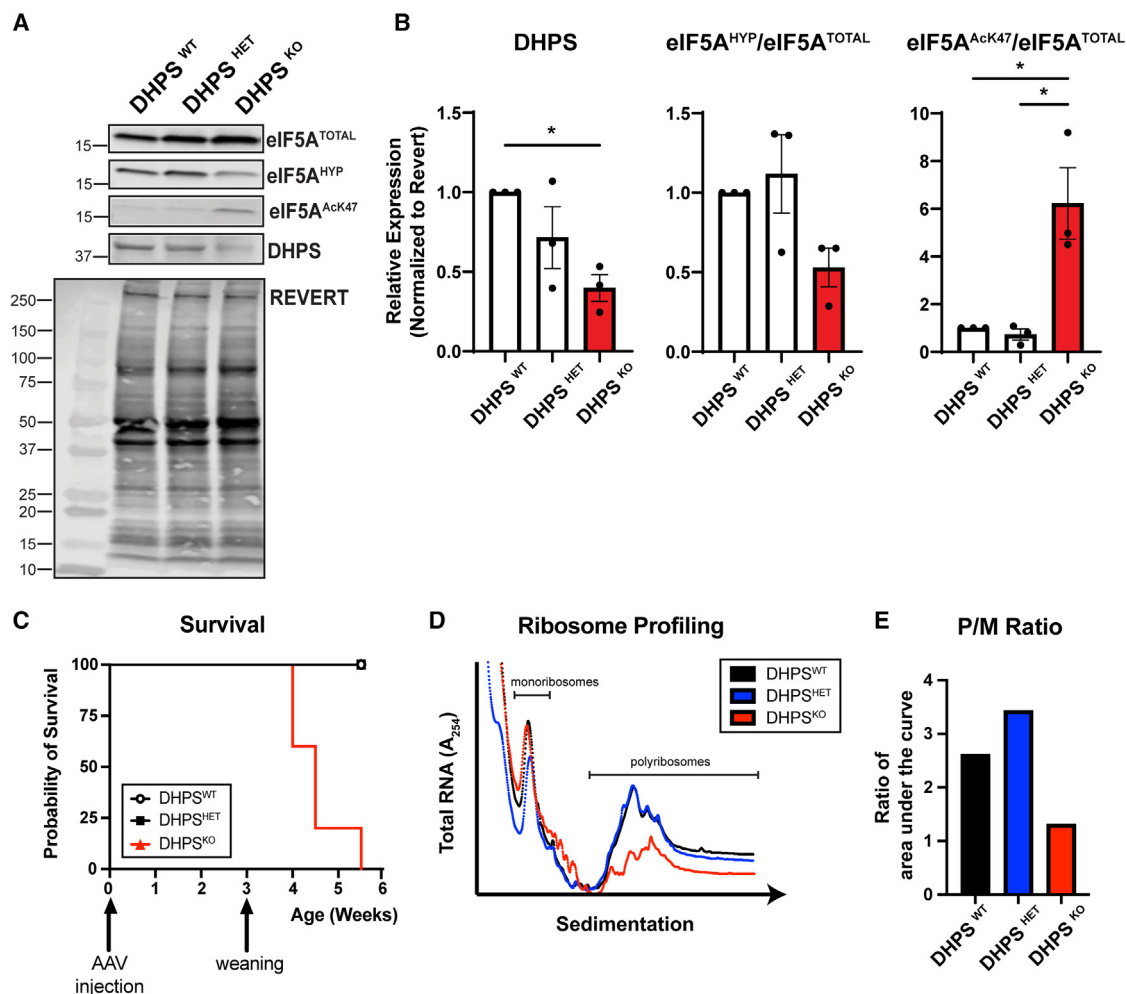


Figure 4. Brain-specific deletion of *Dhps* results in a shift in the abundance of modified forms of eIF5A and altered mRNA translation (A) Representative western blot analysis of brain lysates from *Dhps*^{+/+} (DHPS^{WT}), *Dhps*^{loxP/+} (DHPS^{HET}), and *Dhps*^{loxP/loxP} (DHPS^{KO}) animals, all injected with scAAV2/9-CMV-Cre at birth. Brain tissue from 3-week-old animals was evaluated for expression of DHPS, eIF5A^{HYP}, eIF5A^{TOTAL}, eIF5A^{AcK47}, and REVERT (total protein). Molecular marker notations are in kDa. (B) Densitometric data showing relative expression of DHPS, eIF5A^{HYP}/eIF5A^{TOTAL}, and eIF5A^{AcK47}/eIF5A^{TOTAL} from brain lysate in mutants and controls. Data are means \pm SEM, n = 3; *p < 0.05. (C) The scAAV2/9-CMV-Cre injected DHPS^{WT} (n = 3), DHPS^{HET} (n = 3), and DHPS^{KO} (n = 5) animals were followed for survival and DHPS^{KO} mutant animals died before age 6 weeks. (D) Ribosome profiles measured from brain tissue DHPS^{WT}, DHPS^{HET}, and DHPS^{KO} animals. The monoribosome and polyribosome regions are noted. (E) Quantification of the polyribosome to monoribosome (P/M) area under the curve shows a reduction in the DHPS^{KO}.

in DHPS^{KO} animals compared with DHPS^{WT} and DHPS^{HET} animals (Figures S4C and S4D). Ribosome profiling uses a sucrose gradient to separate mRNA-ribosome complexes based on the number of associated ribosomes. Brain tissue from 3-week-old animals was treated with cycloheximide to stabilize the mRNA-ribosome complexes *in situ*; this lysate was then centrifuged through a sucrose gradient to separate the transcripts based on the rate of sedimentation. The abundance of mRNAs in the monoribosome and polyribosome fractions was quantified. Compared with brain tissue from DHPS^{WT} and DHPS^{HET} animals, ribosome profiles from brain tissue of DHPS^{KO} animals showed a decrease in the polyribosome fractions (Figure 4D). Quantification of the monoribosome and polyribosome area under the curve for each sample revealed a reduced P/M ratio (Figure 4E).

An observed decrease in the polyribosome fraction indicates a reduction in the number of mRNA transcripts undergoing translation, suggesting a reduction in protein synthesis. Therefore, to determine in an unbiased manner the proteins whose synthesis is altered in the absence of *Dhps* in the brain, we used quantitative mass spectrometry to measure unbiased proteomic changes. Overall, this analysis detected 4,592 proteins. The comparison of brain tissue from scAAV2/9-CMV-Cre-injected DHPS^{WT} controls and DHPS^{KO} mutants identified 116 significantly DEPs (p < 0.05; logFC > 1.5), both up- and downregulated (Figure S5). Molecular pathway analysis further revealed alterations in numerous pathways critical for neuronal growth and function including those related to dendrite extension, neurotransmitter synapse, and neuron

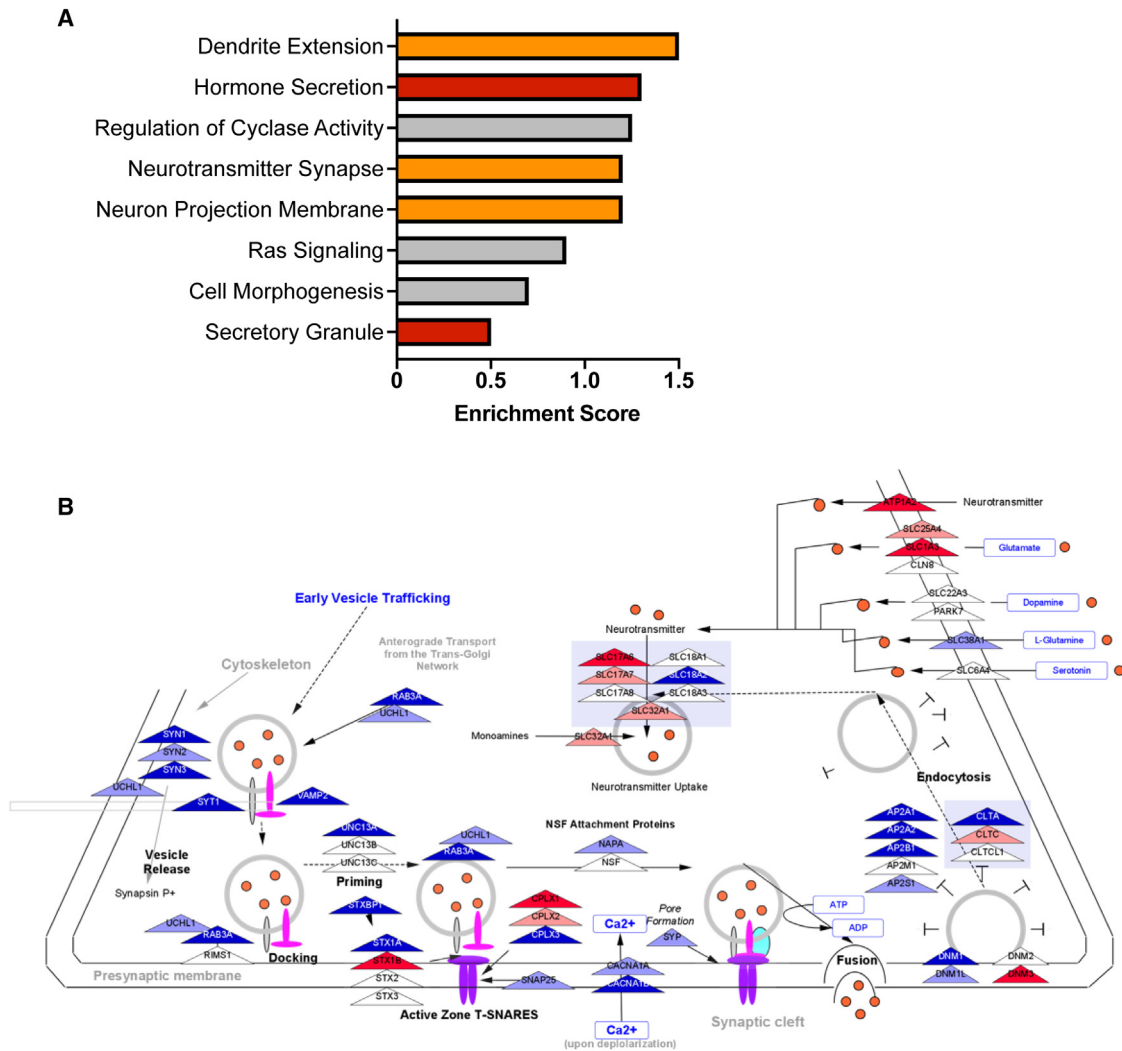


Figure 5. Differentially abundant proteins critical for neuronal function identified in the absence of *Dhps* in the brain (A) Protein set enrichment analysis revealed differentially abundant proteins between the $DHPS^{KO}$ and $DHPS^{WT}$ groups enrich for neuronal (orange) and secretory (red) pathways, as well as cellular signaling processes (gray), using the STRING database. (B) A diagrammatic representation of the synapse of a neuron and the proteins that are downregulated (blue) and upregulated (red) in the $DHPS^{KO}$ compared with the $DHPS^{WT}$, which play a role in neuronal function.

projection membrane (Figure 5A). Furthermore, a significant number of up- and downregulated proteins specifically function in neuronal secretion (Figure 5B). Although this mouse model with deletion of *Dhps* in the brain is similar but not directly equivalent to the biallelic variants in patients with *DHPS* deficiency, our data suggest that altered *DHPS* activity results in decreased $eIF5A^{HYP}$ and altered mRNA translation, which directly impacts the synthesis of proteins critical for proper neuronal function.

Discussion

DHPS deficiency is caused by biallelic hypomorphic variants in the *DHPS* gene, which result in developmental delay, intellectual disability, and seizures. To increase our understanding of this rare genetic disease, it is critical to determine the mechanisms by which mutations in *DHPS*

alter neurodevelopment. In this study, we demonstrate that the human genetic *DHPS* variants associated with this disease alter *DHPS* protein abundance and impair enzyme function. The outcome we observe is a shift in the abundance of the post-translationally modified forms of $eIF5A$ —increasing the acetylated form ($eIF5A^{AcK47}$) and concomitantly decreasing the hypusinated form ($eIF5A^{HYP}$). As the acetylated form is located in the nucleus, this sequesters $eIF5A$ in this compartment resulting in the inability for $eIF5A$ to perform its mRNA translation function in the cytoplasm. In line, our mouse model with a genetic deletion of *Dhps* in the brain at birth shows that loss of hypusine biosynthesis impacts neuronal function due to impaired mRNA translation that causes an altered synthesis of specific proteins required for proper neuronal development and function.

Studies in mice have shown that both complete loss of *Dhps* and conditional loss of *Dhps* during embryonic

development have a dramatic impact on early growth, resulting in either embryonic lethality or impaired organ development and reduced postnatal survival, respectively.^{2,3,13,22} In contrast, our first report on DHPS deficiency established that human hypomorphic mutations in *DHPS* do not impact overall viability but reduce enzyme abundance and function.¹ Clearly, the initial study of DHPS deficiency refined our understanding of the threshold for DHPS activity required for viability. However, the studies herein have advanced this work by determining that, although DHPS protein abundance is altered between biallelic mutant-, carrier-, and control-derived LCLs, relative mRNA expression remains unchanged. Thus, significantly reduced DHPS abundance in carrier cell lines can be attributed to the human DHPS^{SPLICE} and DHPS^{DEL} variants causing DHPS enzyme to be truncated or degraded by the proteasome, respectively.

Interestingly, we observed no significant change in the protein abundance of DHPS in cells from affected individuals with the biallelic DHPS^{MIS}/DHPS^{SPLICE} variants. We speculate that the “wild-type” level abundance of DHPS protein in the DHPS^{MIS}/DHPS^{SPLICE} variant cells may represent a cellular upregulation to compensate for the reduced enzyme activity. Alternatively, the abundance of DHPS in the DHPS^{MIS}/DHPS^{SPLICE} variant cells may derive solely from the presence of the DHPS^{MIS} variant given that DHPS^{SPLICE} carrier cells show reduced abundance of DHPS. However, in either scenario the abundance of DHPS protein does not translate to enzyme activity. Rather, additional data from our 2D gel analysis confirmed that the presence of mutant enzyme ultimately causes a downstream change in the abundance of the hypusinated and acetylated forms of eIF5A. Therefore, the mRNA translation defect and resultant altered protein synthesis come as a direct result of increased eIF5A^{AcK47} and decreased eIF5A^{HYP}. Specifically, eIF5A^{AcK47} is localized to the nucleus and, without the ability to be hypusinated, will never translocate to the cytoplasm and perform its function in mRNA translation. Not much is known about the function of eIF5A^{AcK47} in the nucleus, including whether this modified form is active or inactive thus highlighting the need for further investigation into the functional role of eIF5A^{AcK47}.

Acknowledging the limitation that a mouse model with a genetic deletion of *Dhps* in the brain will not identically model the reported clinical features of DHPS deficiency, the *in vivo* phenotypic data from our mouse model of brain-specific *Dhps* loss showed important similarities. In particular, some of the cellular and clinical phenotypes in the DHPS^{KO} mouse were also observed in the patient-derived LCLs and the individuals with DHPS deficiency, including reduced DHPS and eIF5A^{HYP}, and increased eIF5A^{AcK47} abundance, decreased whole-body growth, and seizures. Therefore, this model can assist with guiding our understanding of the cellular mechanisms that may be interrupted in DHPS deficiency. To that end, cellular analysis of brains from the DHPS^{KO} mice revealed a block in mRNA translation, which is in line with the sequestration of the acetylated form of eIF5A in the nucleus, away

from active ribosomes in the cytoplasm, thus reducing the ability for the mRNA translation function of eIF5A to be performed. Our proteomic analysis subsequently identified many downregulated proteins that function in neuronal growth and secretion. These data, along with the decreased survival in the DHPS^{KO} mice, suggests that eIF5A is required for the translation of genes needed for normal neuronal function. Moreover, in our mouse model, the timing of *Dhps* deletion being on the day of birth suggests that DHPS activity, and therefore proper hypusine biosynthesis, is critical in the perinatal brain to allow for neuronal development and function. Without activation (hypusination) by DHPS, eIF5A may be unable to facilitate the translation of genes required for effective neuronal communication, leading to developmental delay and seizures, which are observed clinical outcomes for individuals with DHPS deficiency.

Overall, our studies illustrate that *DHPS* mutations result in a reduction of eIF5A^{HYP}, which is found in the cytoplasm, and an increase of eIF5A^{AcK47} located in the nucleus thereby causing impaired mRNA translation and altered synthesis of proteins involved in neurodevelopment. Interestingly, unlike other embryonic mouse models of *Dhps* genetic loss that have shown embryonic lethality or diminished organ development,^{2,3,13,22} the clinical findings of individuals with DHPS deficiency demonstrate that neurons do form but may not develop correctly or function appropriately. Furthermore, a genetic model of deletion of *Dhps* in the adult postnatal brain was viable but showed deficiencies in learning and memory.²² Therefore with each animal model of *Dhps* loss we are better understanding its role during development, organogenesis, and in postnatal life.

The discrepancy in phenotypes between the mouse models and the human clinical condition also suggests that there is a minimum level of DHPS/eIF5A^{HYP} that is needed during embryonic development for viability and proper organ development/function. The original *in vitro* analysis of the human *DHPS* variants in the study by Ganapathi et al.¹ showed that this critical threshold may be approximately 20%, such that if the level of DHPS activity (due to mutation) falls below this level, then the organism is not viable. Given that human *DHPS* mutation carriers appear clinically healthy, we can speculate that 50% activity may be sufficient for normal cellular function. These insights raise an important question: if it is possible to increase DHPS activity in the neurons of individuals with DHPS deficiency to 50% that of healthy controls even in the perinatal or adult stages of growth, could this restore the translation of critical proteins and correct some of the impaired neuronal function? This strategy may also prove effective when considering treatments for other related rare human diseases that directly affect eIF5A or hypusine biosynthesis.^{41,42} Moreover, it remains unknown what impact dysfunctional DHPS has on eIF5A2, the homolog of eIF5A1, and the only other human isoform known to be hypusinated by DHPS.⁴³ Ongoing studies are developing animal models with biallelic mutations in the human *DHPS*

gene to more accurately determine the molecular basis for the phenotypes observed in DHPS deficiency as well as develop therapeutic strategies to improve the quality of life for individuals with this rare disease.

Supplemental information

Supplemental information can be found online at <https://doi.org/10.1016/j.xhgg.2023.100206>.

Acknowledgments

The authors would like to thank Patricia Lanzano for technical assistance with creation of the lymphoblast cell lines, Catharina Villaca for technical assistance with image analysis software, and Drs. Nicolas Berbari, Meeta Pradhan, and Dan Robertson for thoughtful discussions. We would also like to acknowledge that mass spectrometry analysis was provided by the Indiana University School of Medicine Proteomics Core Facility. This work was supported by funding to T.L.M. from the DHPS Foundation, the Juvenile Diabetes Research Foundation (JDRF) (5-CDA-2016-194-A-N), and the National Institute of Diabetes and Digestive and Kidney Diseases, National Institutes of Health (NIH) (R01DK121987); funding to M.H.P. from the intramural program of National Institute of Dental and Craniofacial Research, NIH; and funding to R.A.C. and T.M.S. from the Chan Zuckerberg Rare-as-One Initiative/Snyder-Robinson Foundation and University of Pennsylvania Orphan Disease Center Million Dollar Bike Ride (MDBR-20-135-SRS).

Author contributions

T.L.M. and L.R.P. designed the study. L.R.P., M.R.S., S.R., T.M.S., J.R.F., and T.L.M. performed the research. L.R.P., M.R.S., S.R., T.M.S., J.R.F., R.A.C., M.H.P., W.K.C., and T.L.M. analyzed data. L.R.P., M.R.S., and T.L.M. wrote the paper. All authors edited and approved the final draft of the manuscript.

Declaration of interests

W.K.C. is on the Board of Directors for Prime Medicine and on the Scientific Advisory Board for the Regeneron Genetics Center.

Received: January 12, 2023

Revised: May 11, 2023

Accepted: May 15, 2023

Web resources

QuPath software v.0.4.1, <https://qupath.github.io/>.

PCAtools package in R, <https://bioc.ism.ac.jp/packages/3/11/bioc/vignettes/PCAtools/inst/doc/PCAtools.html>.

EnhancedVolcano, <https://bioconductor.org/packages/devel/bioc/vignettes/EnhancedVolcano/inst/doc/EnhancedVolcano.html>.

References

- Ganapathi, M., Padgett, L.R., Yamada, K., Devinsky, O., Willaert, R., Person, R., Au, P.-Y.B., Tagoe, J., McDonald, M., Karłowicz, D., et al. (2019). Recessive rare variants in deoxyhypusine synthase, an enzyme involved in the synthesis of hypusine, are associated with a neurodevelopmental disorder. *Am. J. Hum. Genet.* *104*, 287–298. <https://doi.org/10.1016/j.ajhg.2018.12.017>.
- Templin, A.T., Maier, B., Nishiki, Y., Tersey, S.A., and Mirmira, R.G. (2011). Deoxyhypusine synthase haploinsufficiency attenuates acute cytokine signaling. *Cell Cycle* *10*, 1043–1049.
- Nishimura, K., Lee, S.B., Park, J.H., and Park, M.H. (2012). Essential role of eIF5A-1 and deoxyhypusine synthase in mouse embryonic development. *Amino Acids* *42*, 703–710. <https://doi.org/10.1007/s00726-011-0986-z>.
- Pendeville, H., Carpino, N., Marine, J.C., Takahashi, Y., Muller, M., Martial, J.A., and Cleveland, J.L. (2001). The ornithine decarboxylase gene is essential for cell survival during early murine development. *Mol. Cell Biol.* *21*, 6549–6558.
- Pegg, A.E. (2016). Functions of polyamines in mammals. *J. Biol. Chem.* *291*, 14904–14912. <https://doi.org/10.1074/jbc.R116.731661>.
- Mastracci, T.L., Robertson, M.A., Mirmira, R.G., and Anderson, R.M. (2015). Polyamine biosynthesis is critical for growth and differentiation of the pancreas. *Sci. Rep.* *5*, 13269. <https://doi.org/10.1038/srep13269>.
- Robertson, M.A., Padgett, L.R., Fine, J.A., Chopra, G., and Mastracci, T.L. (2020). Targeting polyamine biosynthesis to stimulate beta cell regeneration in zebrafish. *Islets* *12*, 99–107. <https://doi.org/10.1080/19382014.2020.1791530>.
- Schuller, A.P., Wu, C.C.-C., Dever, T.E., Buskirk, A.R., and Green, R. (2017). eIF5A functions globally in translation elongation and termination. *Mol. Cell* *66*, 194–205.e5. <https://doi.org/10.1016/j.molcel.2017.03.003>.
- Gutierrez, E., Shin, B.S., Woolstenhulme, C.J., Kim, J.R., Saini, P., Buskirk, A.R., and Dever, T.E. (2013). eIF5A promotes translation of polyproline motifs. *Mol. Cell* *51*, 35–45. <https://doi.org/10.1016/j.molcel.2013.04.021>.
- Saini, P., Eyler, D.E., Green, R., and Dever, T.E. (2009). Hypusine-containing protein eIF5A promotes translation elongation. *Nature* *459*, 118–121. <https://doi.org/10.1038/nature08034>.
- Dever, T.E., and Green, R. (2012). The elongation, termination, and recycling phases of translation in eukaryotes. *Cold Spring Harb. Perspect. Biol.* *4*, a013706. <https://doi.org/10.1101/cshperspect.a013706>.
- Gregio, A.P.B., Cano, V.P.S., Avaca, J.S., Valentini, S.R., and Zanelli, C.F. (2009). eIF5A has a function in the elongation step of translation in yeast. *Biochem. Biophys. Res. Commun.* *380*, 785–790. <https://doi.org/10.1016/j.bbrc.2009.01.148>.
- Padgett, L.R., Robertson, M.A., Anderson-Baucum, E.K., Connors, C.T., Wu, W., Mirmira, R.G., and Mastracci, T.L. (2021). Deoxyhypusine synthase, an essential enzyme for hypusine biosynthesis, is required for proper exocrine pancreas development. *FASEB J* *35*, e21473. <https://doi.org/10.1096/fj.201903177R>.
- Park, M.H., Cooper, H.L., and Folk, J.E. (1981). Identification of hypusine, an unusual amino acid, in a protein from human lymphocytes and of spermidine as its biosynthetic precursor. *Proc. Natl. Acad. Sci. USA* *78*, 2869–2873.
- Park, J.-H., Aravind, L., Wolff, E.C., Kaevel, J., Kim, Y.S., and Park, M.H. (2006). Molecular cloning, expression, and structural prediction of deoxyhypusine hydroxylase: a HEAT-repeat-containing metalloenzyme. *Proc. Natl. Acad. Sci. USA* *103*, 51–56. <https://doi.org/10.1073/pnas.0509348102>.

16. Kemper, W.M., Berry, K.W., and Merrick, W.C. (1976). Purification and properties of rabbit reticulocyte protein synthesis initiation factors M2Balpha and M2Bbeta. *J. Biol. Chem.* *251*, 5551–5557.
17. Benne, R., Brown-Laeter, M.L., and Hershey, J.W. (1978). Purification and characterization of protein synthesis initiation factors eIF-1, eIF-4C, eIF-4D, and eIF-5 from rabbit reticulocytes. *J. Biol. Chem.* *253*, 3070–3077.
18. Igarashi, K., and Kashiwagi, K. (2010). Modulation of cellular function by polyamines. *Int. J. Biochem. Cell Biol.* *42*, 39–51. <https://doi.org/10.1016/j.biocel.2009.07.009>.
19. Igarashi, K., and Kashiwagi, K. (2019). The functional role of polyamines in eukaryotic cells. *Int. J. Biochem. Cell Biol.* *107*, 104–115. <https://doi.org/10.1016/j.biocel.2018.12.012>.
20. Sievert, H., Pällmann, N., Miller, K.K., Hermans-Borgmeyer, I., Venz, S., Sendoel, A., Preukschas, M., Schweizer, M., Boettcher, S., Janiesch, P.C., et al. (2014). A novel mouse model for inhibition of DOHH-mediated hypusine modification reveals a crucial function in embryonic development, proliferation and oncogenic transformation. *Dis. Model. Mech.* *7*, 963–976. <https://doi.org/10.1242/dmm.014449>.
21. Levasseur, E.M., Yamada, K., Piñeros, A.R., Wu, W., Syed, F., Orr, K.S., Anderson-Baucum, E., Mastracci, T.L., Maier, B., Mosley, A.L., et al. (2019). Hypusine biosynthesis in β cells links polyamine metabolism to facultative cellular proliferation to maintain glucose homeostasis. *Sci. Signal.* *12*, eaax0715. <https://doi.org/10.1126/scisignal.aax0715>.
22. Kar, R.K., Hanner, A.S., Starost, M.F., Springer, D., Mastracci, T.L., Mirmira, R.G., and Park, M.H. (2021). Neuron-specific ablation of eIF5A or deoxyhypusine synthase leads to impairments in growth, viability, neurodevelopment, and cognitive functions in mice. *J. Biol. Chem.* *297*, 101333. <https://doi.org/10.1016/j.jbc.2021.101333>.
23. Huang, Y., Higginson, D.S., Hester, L., Park, M.H., and Snyder, S.H. (2007). Neuronal growth and survival mediated by eIF5A, a polyamine-modified translation initiation factor. *Proc. Natl. Acad. Sci. USA* *104*, 4194–4199. <https://doi.org/10.1073/pnas.0611609104>.
24. Maier, B., Ogihara, T., Trace, A.P., Tersey, S.A., Robbins, R.D., Chakrabarti, S.K., Nunemaker, C.S., Stull, N.D., Taylor, C.A., Thompson, J.E., et al. (2010). The unique hypusine modification of eIF5A promotes islet beta cell inflammation and dysfunction in mice. *J. Clin. Invest.* *120*, 2156–2170. <https://doi.org/10.1172/JCI38924>.
25. Meleady, P. (2018). Two-dimensional gel electrophoresis and 2D-DIGE. *Methods Mol. Biol.* *1664*, 3–14. https://doi.org/10.1007/978-1-4939-7268-5_1.
26. Dhir, H., Choudhury, M., Patil, K., Cheung, C., Bodlak, A., Pardo, D., Adams, A., Travaglino, S., Rojas, J.A., and Pai, S.B. (2021). Interception of signaling circuits of esophageal adenocarcinoma cells by resveratrol reveals molecular and immunomodulatory signatures. *Cancers* *13*, 5811. <https://doi.org/10.3390/cancers13225811>.
27. Huang, H., Dabrazhynetskaya, A., Pluznik, J., Zheng, J., Wu, Y., Chizhikov, V., Buehler, P.W., Yamada, K.M., and Dhawan, S. (2021). Hemin activation abrogates Mycoplasma hyorhinis replication in chronically infected prostate cancer cells via heme oxygenase-1 induction. *FEBS Open Bio* *11*, 2727–2739. <https://doi.org/10.1002/2211-5463.13271>.
28. Kabra, P.M., Lee, H.K., Lubich, W.P., and Marton, L.J. (1986). Solid-phase extraction and determination of dansyl derivatives of unconjugated and acetylated polyamines by reversed-phase liquid chromatography: improved separation systems for polyamines in cerebrospinal fluid, urine and tissue. *J. Chromatogr.* *380*, 19–32. [https://doi.org/10.1016/s0378-4347\(00\)83621-x](https://doi.org/10.1016/s0378-4347(00)83621-x).
29. Madisen, L., Zwingman, T.A., Sunkin, S.M., Oh, S.W., Zariwala, H.A., Gu, H., Ng, L.L., Palmiter, R.D., Hawrylycz, M.J., Jones, A.R., et al. (2010). A robust and high-throughput Cre reporting and characterization system for the whole mouse brain. *Nat. Neurosci.* *13*, 133–140. <https://doi.org/10.1038/nn.2467>.
30. Bankhead, P., Loughrey, M.B., Fernández, J.A., Dombrowski, Y., McArt, D.G., Dunne, P.D., McQuaid, S., Gray, R.T., Murray, L.J., Coleman, H.G., et al. (2017). QuPath: open source software for digital pathology image analysis. *Sci. Rep.* *7*, 16878. <https://doi.org/10.1038/s41598-017-17204-5>.
31. Hatanaka, M., Maier, B., Sims, E.K., Templin, A.T., Kulkarni, R.N., Evans-Molina, C., and Mirmira, R.G. (2014). Palmitate induces mRNA translation and increases ER protein load in islet β -cells via activation of the mammalian target of rapamycin pathway. *Diabetes* *63*, 3404–3415. <https://doi.org/10.2337/db14-0105>.
32. Iovosev, G., Burton, L., and Bonner, R. (2008). Dimensionality reduction and visualization in principal component analysis. *Anal. Chem.* *80*, 4933–4944. <https://doi.org/10.1021/ac800110w>.
33. Ritchie, M.E., Phipson, B., Wu, D., Hu, Y., Law, C.W., Shi, W., and Smyth, G.K. (2015). Limma powers differential expression analyses for RNA-sequencing and microarray studies. *Nucleic Acids Res.* *43*, e47. <https://doi.org/10.1093/nar/gkv007>.
34. van Ooijen, M.P., Jong, V.L., Eijkemans, M.J.C., Heck, A.J.R., Andeweg, A.C., Binai, N.A., and van den Ham, H.-J. (2018). Identification of differentially expressed peptides in high-throughput proteomics data. *Brief. Bioinform.* *19*, 971–981. <https://doi.org/10.1093/bib/bbx031>.
35. Kammers, K., Cole, R.N., Tiengwe, C., and Ruczinski, I. (2015). Detecting significant changes in protein abundance. *EuPA Open Proteom.* *7*, 11–19. <https://doi.org/10.1016/j.euprot.2015.02.002>.
36. Szklarczyk, D., Gable, A.L., Nastou, K.C., Lyon, D., Kirsch, R., Pyysalo, S., Doncheva, N.T., Legeay, M., Fang, T., Bork, P., et al. (2021). The STRING database in 2021: customizable protein-protein networks, and functional characterization of user-uploaded gene/measurement sets. *Nucleic Acids Res.* *49*, D605–D612. <https://doi.org/10.1093/nar/gkaa1074>.
37. Kim, J.A., Vetrivel, P., Kim, S.M., Ha, S.E., Kim, H.H., Bhosale, P.B., Heo, J.D., Lee, W.S., Senthil, K., and Kim, G.S. (2021). Quantitative proteomics analysis for the identification of differential protein expression in calf muscles between young and old SD rats using mass spectrometry. *ACS Omega* *6*, 7422–7433. <https://doi.org/10.1021/acsomega.0c05821>.
38. Slenter, D.N., Kutmon, M., Hanspers, K., Riutta, A., Windsor, J., Nunes, N., Mélius, J., Cirillo, E., Coort, S.L., Digles, D., et al. (2018). WikiPathways: a multifaceted pathway database bridging metabolomics to other omics research. *Nucleic Acids Res.* *46*, D661–D667. <https://doi.org/10.1093/nar/gkx1064>.
39. Shannon, P., Markiel, A., Ozier, O., Baliga, N.S., Wang, J.T., Ramage, D., Amin, N., Schwikowski, B., and Ideker, T. (2003). Cytoscape: a software environment for integrated models of biomolecular interaction networks. *Genome Res.* *13*, 2498–2504. <https://doi.org/10.1101/gr.1239303>.
40. Ishfaq, M., Maeta, K., Maeda, S., Natsume, T., Ito, A., and Yoshida, M. (2012). Acetylation regulates subcellular

- localization of eukaryotic translation initiation factor 5A (eIF5A). *FEBS Lett.* 586, 3236–3241. <https://doi.org/10.1016/j.febslet.2012.06.042>.
41. Ziegler, A., Steindl, K., Hanner, A.S., Kar, R.K., Prouteau, C., Boland, A., Deleuze, J.F., Coubes, C., Bézieau, S., Küry, S., et al. (2022). Bi-allelic variants in DOHH, catalyzing the last step of hypusine biosynthesis, are associated with a neurodevelopmental disorder. *Am. J. Hum. Genet.* 109, 1549–1558. <https://doi.org/10.1016/j.ajhg.2022.06.010>.
42. Faundes, V., Jennings, M.D., Crilly, S., Legraie, S., Withers, S.E., Cuvertino, S., Davies, S.J., Douglas, A.G.L., Fry, A.E., Harrison, V., et al. (2021). Impaired eIF5A function causes a Mendelian disorder that is partially rescued in model systems by spermidine. *Nat. Commun.* 12, 833. <https://doi.org/10.1038/s41467-021-21053-2>.
43. Wu, G.-Q., Xu, Y.-M., and Lau, A.T.Y. (2020). Recent insights into eukaryotic translation initiation factors 5A1 and 5A2 and their roles in human health and disease. *Cancer Cell Int.* 20, 142. <https://doi.org/10.1186/s12935-020-01226-7>.